Defects on SPECT "Perfusion" Images Can Occur Due to Abnormal Segmental Contraction

Robert L. Eisner, L. Susan Schmarkey, Sharon E. Martin, Daniel Carey, Marquis A. Worthy, Tsann H. Chu, Steven F. Horowitz and Randolph E. Patterson

Carlyle Fraser Heart Center, Emory/Crawford Long Hospital; Departments of Radiology, Medicine (Cardiology) and Physiology, Emory University School of Medicine, Atlanta, Georgia; and Department of Medicine (Cardiology), Beth Israel Medical Center, Mt. Sinai School of Medicine, New York, New York

Technetium-99m-sestamibi images reflect tracer distribution at the time of injection. This "stay put" indicator allowed us to separate the effects of segmental left ventricular dysfunction per se versus myocardial blood flow on SPECT "perfusion" images in ten dogs. **Methods:** An electromagnetic flow probe and hydraulic occluder were placed on the LAD coronary artery. Sonomicrometry was used to measure segmental wall shortening. At peak myocardial blood flow induced by adenosine, 35–45 mCi ^{99m}Tc-sestamibi were injected without occlusion. At 1 hr postinjection, during normal contraction, 40–50 msec end-diastolic and end-systolic SPECT images (#1) were acquired to reflect normal myocardial blood flow distribution. Later, during total LAD occlusion, and without reinjection of isotope, another gated scan (#2) was acquired. **Results:** Coincident with abnormal contraction, large severe systolic defects [(28 ± 5)% more severe compared to the baseline-scan #1; $p < 0.01$], and milder diastolic defects [(12 ± 8)% more severe compared to the baseline-scan #1; $p < 0.01$] were observed during scan #2. Thus, abnormal contraction alone produced defects on SPECT images. **Conclusion:** Accordingly, defects in myocardial perfusion images must be interpreted as representing the integrated result of the combination of blood flow and segmental contraction heterogeneity.

Key Words: SPECT myocardial perfusion imaging; gated SPECT; technetium-99m-sestamibi

J Nucl Med 1994; 35:638–643

If coronary blood flow reserve is limited by partial coronary occlusion, then exercise can produce myocardial ischemia manifested by chest discomfort, electrocardiographic (ECG) ST-segment depression, decreased regional myocardial perfusion and impaired regional cardiac contraction (*1*). Injection of ^{201}Tl or ^{99m}Tc-hexakis-2-methoxy-2-methyl isobutyl isonitrile (sestamibi) during exercise allows imaging of myocardial perfusion for a few minutes (^{201}Tl) or hours (^{99m}Tc-sestamibi) later, even though actual coronary blood flow distribution returns toward normal (*2*). Regional cardiac contraction, on the other hand, returns toward normal more slowly after a brief period of ischemia due to myocardial "stunning" (*3*). Therefore, image acquisition may occur while regional contraction is potentially still significantly impaired.

The objective of the present study was to determine whether abnormal segmental contraction per se could influence the appearance of SPECT myocardial perfusion images. The work of Gewirtz et al. (*4*) described the effects of changes in regional contraction and left ventricular geometry on ungated and gated planar myocardial perfusion images. Parodi et al. (*5*) studied the influence of abnormal regional contraction on ungated PET images. Myocardial perfusion images are normally acquired in a nongated fashion which blurs systole and diastole (*6*). In our design, the images were gated in order to avoid the concomitant effects of overall global cardiac motion in space associated with the cardiac cycle. We then were able to determine the effects of changes in regional function.

Technetium-99m-sestamibi shows little redistribution so that images reflect the same, initial tracer distribution for several hours (*7–9*). We took advantage of the ^{99m}Tc-sestamibi "stay-put" property and acquired multiple ECG-gated SPECT ^{99m}Tc-myocardial perfusion images under different conditions of regional left ventricular contraction following a single injection of ^{99m}Tc-sestamibi. Dogs were instrumented to record coronary blood flow by an electromagnetic flow probe and segmental shortening by ultrasonic crystals as a "gold standard" measurement of local myocardial contraction. Following instrumentation, each dog then received ^{99m}Tc-sestamibi during adenosine "stress." One hour later, without reinjection of isotope, ECG-gated images at diastole and systole were acquired at rest (normal systolic contractile function), and still later, during total coronary artery occlusion (diminished or absent systolic contractile function in the myocardial region supplied by the occluded coronary artery). The experimental design allowed us to infer that any differences in the severity and extent of "perfusion" defects between the baseline resting perfusion scans and the scans acquired during occlusion in the same dog were related to changes in

Received Jul. 19, 1993; revision accepted Dec. 29, 1993.

For correspondence or reprints contact: Robert L. Eisner, PhD, Carlyle Fraser Heart Center, Emory/Crawford Long Hospital, Department of Nuclear Cardiology, 550 Peachtree St., NE, Atlanta, GA 30365.

regional left ventricular contraction, and not to changes in ^{99m}Tc-sestamibi measurements of myocardial "perfusion" per se since ^{99m}Tc-sestamibi had already been deposited in the myocardium.

METHODS

Experimental Preparation

Ten mongrel dogs weighing 20 to 35 kg were premedicated with acepromazine (8 mg, s.c.). Methohexital (11 mg · kg^{-1}) and alpha-chloralose (100 mg · kg^{-1}) were given as intravenous boluses. Anesthesia was maintained by a constant intravenous infusion of 5 to 8 mg · kg^{-1} · hr^{-1} of alpha-chloralose. The dogs were intubated and mechanically ventilated (Bennett MA-1). Four limb lead electrodes were attached subcutaneously for ECG recording. Catheters were placed in the femoral artery and vein to measure blood pressure and drug infusion, respectively. Later, a high fidelity pressure sensor-tipped catheter (Millar Instruments, Houston, TX) was inserted into the left femoral artery and advanced into the left ventricle to record left ventricular pressure and its first derivative (dP/dt). The chest was opened by left lateral thoracotomy at the fifth intercostal space. An electromagnetic flow probe (Carolina Medical Electronics, King, NC) was placed around the left anterior descending (LAD) coronary artery after careful dissection to avoid coronary occlusion. A hydraulic occluder (In Vivo Metrics, Healdsburg, CA or RE Jones, Co. Silver Springs, MD) was secured around the LAD distal to the electromagnetic flow probe. No studies were performed for at least 1 hr after LAD dissection. Heart rate, systolic, diastolic and mean aortic pressure, dP/dt, mean and phasic coronary blood flow were recorded.

Regional left ventricular segmental shortening was measured from the transit time for ultrasonic crystals implanted in the myocardium (*10–12*). Two crystal pairs were placed, one in the distribution of the LAD (coronary artery with hydraulic occluder) and the other in the distribution of the (normal) left circumflex coronary artery (LCx), and recorded on an ultrasonic dimension system (Triton Technologies, La Jolla, CA). Crystal pairs were positioned to record parallel to the fibers 5 to 7 mm under the surface and to record the largest amplitude signal available. Crystals were placed clearly between branches of the LAD distal to the site of the hydraulic occluder. End-diastolic dimension was identified on ultrasonic crystal tracing as the time when dP/dt started to rise, and the end-systolic dimension as the time 20 msec before peak negative dP/dt (*12*). The percent segmental shortening (SS) was calculated as (100%) × ((end-diastolic length − end-systolic length) divided by (end-diastolic length)). SS has been shown to correlate strongly with systolic wall thickening (*13*). SS was calculated for both the LAD-perfused and LCx-perfused myocardial segments. The percent changes between baseline-rest and occlusion in the end-diastolic (%ΔEDL) and end-systolic (%ΔESL) crystal dimensions were calculated for both the LAD and LCx zones. The %ΔEDL and %ΔESL are measures of LV volumetric changes at diastole and systole, respectively.

Protocols

The chest of each dog was closed surgically, and coronary blood flow was increased to its maximum value with intravenous adenosine. Since the major clinical use of SPECT ^{99m}Tc-sestamibi is stress testing, we infused adenosine to achieve maximum coronary dilatation without altering contractility before radionuclide injection. In a previous study, we found that an intravenous dose of adenosine caused reproducible maximal coronary vasodilation measured by an electromagnetic flow probe in dogs (*14*). Peak levels of coronary blood flow were achieved by intravenous infusion of incremental doses (36–139 μg · kg^{-1} · min^{-1}) of adenosine (5 m*M* in saline). At peak stress in each animal (n = 10), the hydraulic occluder was *not* inflated (i.e., the LAD was patent) and an intravenous injection of 35–45 mCi ^{99m}Tc-sestamibi was given. SPECT ^{99m}Tc-sestamibi acquisitions were performed later under varied conditions of regional contractile function as follows:

- *Baseline-rest scan (#1):* One hour after injection, when crystals and blood flow measurements returned to baseline (i.e., resting) values, ECG-gated SPECT scans of resting, normal conditions were acquired.
- *Occlusion scan (#2):* Later, without moving the dog, a bolus of lidocaine (40 to 60 mg, i.v.) was given, and a slow infusion begun (1 mg · min^{-1}, i.v.) to minimize the occurrence of arrhythmias associated with coronary occlusion. Then, the hydraulic occluder was inflated to produce a total coronary occlusion confirmed by 100% reduction in coronary blood flow. The LAD crystals showed negative or little segmental shortening, as expected with total coronary occlusion. Without reinjection of radioisotope, ECG-gated SPECT ^{99m}Tc-sestamibi imaging began (i.e., during abnormal contraction). The occlusion was maintained throughout the SPECT acquisition.

SPECT Acquisition

Gated Tomographic Acquisition. For each study protocol (#1 and #2), images at diastole and systole were acquired simultaneously. Diastolic images were acquired beginning at the R-wave and for a time interval of 40–50 msec. Systolic images were acquired beginning at 20 msec before the time of "end-systole" as defined by the segment crystals (see above) and for a duration of 40–50 msec. A low-energy, high-resolution (LEHR) collimator was used to enhance SPECT resolution. View data were acquired on a General Electric 400AT/STAR SPECT system using a camera zoom of 1.6 into a 64 × 64 digital matrix (i.e., sampling size equal to 3.9 mm per pixel). Each dataset, consisting of 64 views, was acquired using a circular 180° anterior arc scan. The SPECT acquisition time was kept between 30 to 40 min so that the number of cardiac cycles acquired at each view depended on the experimental conditions during the study (i.e., the dog's heart rate).

Cholecystokinin Infusion. Gallbladder activity can interfere with ^{99m}Tc-sestamibi myocardial images in dogs (*14*). Thus, in three dogs, 50 min after injecting ^{99m}Tc-sestamibi, at which time the tracer was already deposited in the heart and other tissues, synthetic cholecystokinin (1 μg boluses up to 10 μg total; Sincalide, Squibb Laboratories, Princeton, NJ) was injected intravenously to induce gallbladder emptying and clear ^{99m}Tc-sestamibi from the area near the heart as described previously (*14*). Cholecystokinin boluses only transiently altered systemic and coronary hemodynamics, and variables always returned to baseline conditions within 1 min. A cholecystokinin infusion (0.007 μg · min^{-1}) was continued during the SPECT acquisition. In the other seven dogs, a cannula was placed in the gallbladder during surgical instrumentation, and the contents drained periodically over the course of the SPECT acquisitions.

Analysis of SPECT Images. The end-diastolic and end-systolic SPECT ^{99m}Tc-sestamibi scans were processed using the authors' bull's-eye analysis software (*15*). After nine-point smoothing of the planar images, transaxial slices (3.9 mm thick) were reconstructed using ramp-filtered backprojection without attenuation

correction. Following operator definition of the angularity of the heart in the thorax, the slices from the vertical long-axis, horizontal long-axis, and short-axis were reformatted from the transaxial dataset. The ^{99m}Tc-sestamibi short axis slices were passed through the quantitative bull's-eye program where apical to basal slices were selected by an experienced operator. For each animal, the same number of short-axis slices was used for all end-diastolic and end-systolic studies. A maximal count circumferential analysis was performed on each short-axis slice to produce a series of circumferential profiles. For all slices, except for the first two apical slices, the maximum count was determined along 40 radial vectors (i.e., 9° angular increments) emanating from an operator-defined center of the left ventricle. For the first two apical slices, which do not have the doughnut-shaped appearance of the other short-axis slices, the maximum count in the slice was obtained. For display purposes, the circumferential profiles were coalesced into the two-dimensional bull's-eye representation.

A maximal count analysis was performed in spherical coordinates to better describe the count distribution in the apical region of the left ventricle. In this approach, the apical portion of the vertical long-axis slice array was sampled by radial vectors emanating from the operator-defined center at a distance of 20% of the apical to basal extent of the left ventricle. Maximal counts were obtained at five different angular (Θ) intervals (i.e., Θ varied from 0° to 90° in 22.5° steps) with 40 ϕ values (i.e., ϕ varied from 0° to 360° in 9° increments). The apical samples (5 × 40 = 200 values) were displayed in a two-dimensional bull's-eye representation (CAP display) with samples along the line passing through the center of the left ventricle (Θ = 0°) shown at the center of the display.

Quantitative Analysis. In a previous study (*14*), we established a threshold criterion for identification of an abnormally "perfused" region (i.e., defect region). Thus, circumferential profile pixels with counts less than 60% of the maximum count in the study, which were in a region of the circumferential profile correlating anatomically to the "occluded" LAD, were identified as abnormal. When this same threshold criterion was applied to all data in the present study, a significant defect was apparent in *all* the systolic images from the occlusion scan. Thus, we defined the defect region on the end-systolic scan at occlusion and mapped this region to circumferential profile images from all studies in the same animal. The average number of counts in the defect zone was determined from the mapped defect region in each study. In a similar manner, a normal region was standardized for all the animal studies and corresponded to an area perfused predominantly by the nonoccluded LCx coronary artery. This normal region then was mapped to all the studies, and the average number of counts in the normal zone was determined.

Defect severity was defined as the average number of counts per pixel in the defect zone divided by the average number of counts per pixel in the normal zone. The percent change in defect severity from baseline (scan 1) to the occlusion (scan 2) was calculated for diastolic and systolic images.

Results were expressed as the mean ± standard deviation. Comparison of differences in defect severity change between rest and occlusion images were performed by Student's t-test. Differences were considered significant when $p < 0.05$.

Ungated Tomographic Acquisition

Clinically, SPECT myocardial perfusion images are usually acquired in a nongated fashion. Thus, to assess the effects of abnormal segmental contraction on the appearance of ungated images, we acquired ungated SPECT ^{99m}Tc-sestamibi data at baseline-rest and during occlusion in one additional animal. Acquisition and processing parameters were identical to those used in the gated study, except the time/view was fixed at 30 sec.

RESULTS

Qualitative Comparison of SPECT Bull's-eye Images

Baseline-Rest Scan. End-systolic SPECT ^{99m}Tc-sestamibi bull's-eye displays acquired during normal contraction conditions in four representative dogs are seen in the top row of Figure 1 (#1–#4) in which no defects are apparent. The corresponding end-diastolic bull's-eye displays from the same four dogs are shown in the top row of Figure 2. The slight decrease of counts in the anterior and apical sectors in the diastolic images is consistent with our previous observations in normal dogs (*16*).

Occlusion Scan. In contrast to the baseline-rest images, large severe defects are apparent in all end-systolic bull's-eye displays acquired during total coronary occlusion from the same four dogs (row B in Fig. 1). Figure 1, row C (CAP display), magnifies the center of the bull's-eye to show decreased counts in the apical region during occlusion. The blackened area in Figure 1, row D identifies the extent of the defects. The diastolic bull's-eye images (bottom row of Fig. 2) show more variable results. For dogs 2 and 4, defects are less severe and smaller than in the corresponding end-systolic images. For dog 1 defect severity is similar to that in the systolic image, whereas for dog 3 no defect is apparent when compared to the baseline diastolic image (the systolic image for dog 3 shows a large defect).

Qualitative Comparison of SPECT Slices

The differences between images are not only apparent in bull's-eye displays. Figure 3 (columns 1–4) shows a comparison of end-systolic SPECT slices from the four dogs. Transaxial slices (row A) and vertical long-axis slices (row C) acquired during normal contraction conditions are compared to transaxial slices (row B) and vertical long-axis slices (row D) acquired during occlusion. Thus, at the same slice level, there are obvious differences in relative count levels with severe defects during abnormal segmental contraction observed in the anterior, antero-apical and apical regions of the slices displayed in rows B and D (occlusion). In association with the appearance of decreased count levels in these regions, images acquired during occlusion show LV cavity dilation.

Quantitative Comparison

At baseline-rest, segmental shortening was comparable in the LAD-perfused (SS = 14% ± 6%) and the LCx-perfused (SS = 12% ± 5%) regions. During occlusion, SS in the abnormal (LAD) region was negative in 7/10 animals and averaged (−1 ± 6)%. Relative to baseline-rest, SS during occlusion decreased significantly in all studies [average $\%\Delta$ = (−124 ± 65)%]. Since SS has been shown to correlate strongly with systolic wall thickening (*13*), our SS data imply significantly reduced systolic wall thickening in 3/10 studies and paradoxical systolic wall thinning in 7/10

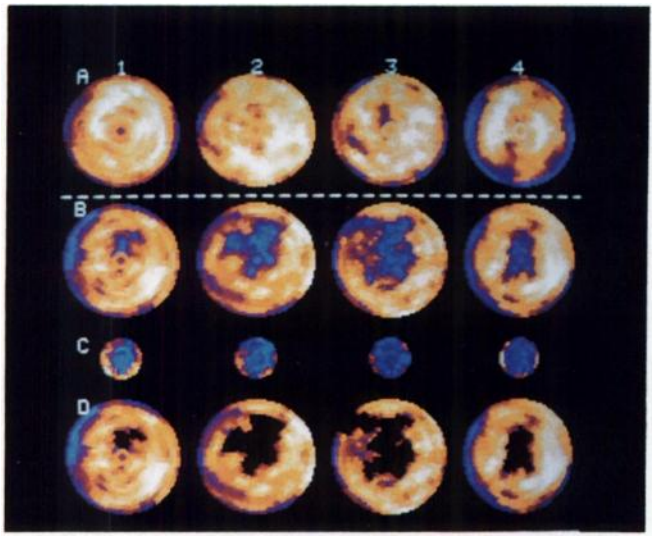

FIGURE 1. End-systolic bull's-eye displays from four representative dogs. From left to right, dogs 1–4 are shown (#1–#4). (Row A) Baseline-rest images were acquired during normal segmental contraction. (Row B) Occlusion images were acquired during abnormal segmental contraction. (Row C) Occlusion images (CAP displays) better sample the apical region to show the apical extent of the defects. (Row D) The same occlusion images displayed in Row B are shown with the defect region shown in black. Abnormal segmental contraction produces a severe defect on occlusion bull's-eye even though coronary blood flow was normal during isotope distribution as reflected by normal baseline-rest images.

studies during occlusion. In the normal LCx zone, SS was decreased slightly [average %Δ = −20% ± 34%], perhaps because of the administration of lidocaine prior to coronary occlusion. Accordingly, during occlusion, systolic wall thickness in the region of the LAD decreased significantly compared to the LCx. The thickness change was associated with a volumetric change, i.e., bulging, in the same LAD-region as shown by a 24% ± 10% increase in the length between crystals (i.e., %ΔESL) during systole. Only minor crystal dimension changes occurred in the same region during diastole (%ΔEDL = 6% ± 6%) or in the LCx region during systole (%ΔESL = 8% ± 15%) and diastole (%ΔEDL = 2% ± 3%). These measurements suggest little change in left ventricular end-diastolic volume during this study.

Figure 4 shows how these changes in segmental wall function between rest and occlusion influence the change in defect severity between the two scans. The figure summarizes our results and shows that severe defects [(28 ± 5)% more severe], compared to baseline scans, are present in the systolic image acquired during total occlusion ($p < 0.01$, baseline versus occlusion). Diastolic images acquired during occlusion show smaller [(12 ± 8)% more severe], but significant, differences when compared to baseline images ($p < 0.01$). In all cases (10/10), defects were observed in the systolic images during occlusion. In (9/10) cases, defects were present, but were less severe at diastole during occlusion ($p < 0.01$, systole versus diastole).

Ungated Scan

For the images acquired without ECG gating, SS in the LAD decreased from 17.6% to −5.7% during occlusion. SS in the LCx increased slightly from 8.2% to 10%. The %ΔESL (LAD) = +49.2%, %ΔEDL (LAD) = +14.4%, %ΔESL (LCx) = −6.4%, and %ΔEDL (LCx) = −8.3%. Thus, as in the ungated data, negative segmental shortening (i.e., systolic wall thinning) in association with a volumetric bulging of the myocardium during systole occurred in the region perfused by the occluded LAD. The baseline-rest bull's-eye display, CAP display and a representative transaxial slice from the ungated acquisition are shown in

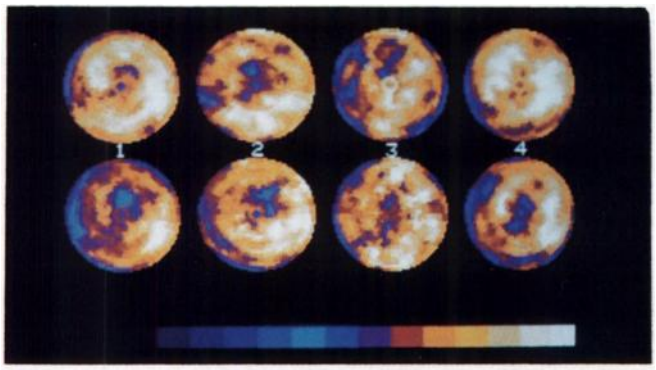

FIGURE 2. End-diastolic bull's-eye displays from the same four dogs shown in Figure 1. (Top row) Baseline-rest images were acquired during normal segmental contraction. (Bottom row) Occlusion images were acquired during abnormal segmental contraction.

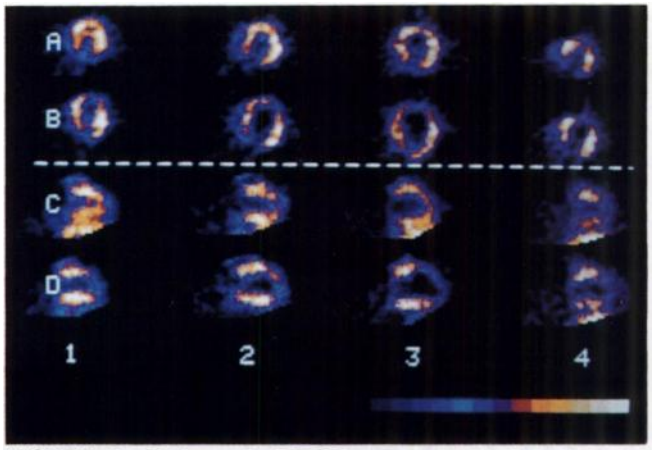

FIGURE 3. End-systolic SPECT reconstructed slices from the same four dogs shown in Figure 1. (Row A) SPECT reconstructed (7.8 mm thick) transaxial slices acquired during normal segmental contraction (baseline-rest). (Row B) At the same slice level, SPECT reconstructed (7.8 mm thick) transaxial slices acquired during abnormal segmental contraction (occlusion). (Row C) Vertical long-axis slices (7.8 mm thick) acquired during normal segmental contraction (baseline-rest). (Row D) At the same slice level, vertical long-axis slices (7.8 mm thick) acquired during abnormal segmental contraction (occlusion). The images have been normalized independently with the maximum count in each image set to the same color (white). Compared to baseline-rest studies, abnormal segmental contraction produces a severe defect during occlusion in the anterior, apical and antero-apical regions.

the top row of Figure 5. Corresponding images acquired during occlusion (bottom row of Fig. 5) show decreased count levels in the anterior, antero-apical and apical segments. Accordingly, the "artifactual" effects of abnormal segmental contraction on SPECT images was also observed in the ungated scan.

DISCUSSION

Prior studies have shown a relationship between global left ventricular function and myocardial perfusion images (*4,5,17*). Gewirtz et al. (*4*) studied the effect of abnormal wall motion on gated and ungated planar images. Parodi et al. (*5*) showed the effect of abnormal function on ungated ^{13}N-ammonia PET images. Machac et al. (*17*) showed a relationship between left ventricular function, cavity size and wall thickness using computer simulations of ^{201}Tl images. Based on these studies, it seemed reasonable to test whether regional contractile abnormalities might alter SPECT myocardial perfusion images. We gated our images to produce "stop-action," thereby avoiding any effects of motion associated with the cardiac cycle on the image. The two-frame gated image used a narrow window of only 40–50 msec during diastole and again in systole. The timing of this systolic window was made quite exact by using a combination of the timing of changes in left ventricular pressure, its first derivative and segmental ultrasonic crystals in the wall of the heart. Thus, we avoided any overlap of diastolic and systolic events during the periods we designated and imaged as "end-diastole" and "end-systole," respectively.

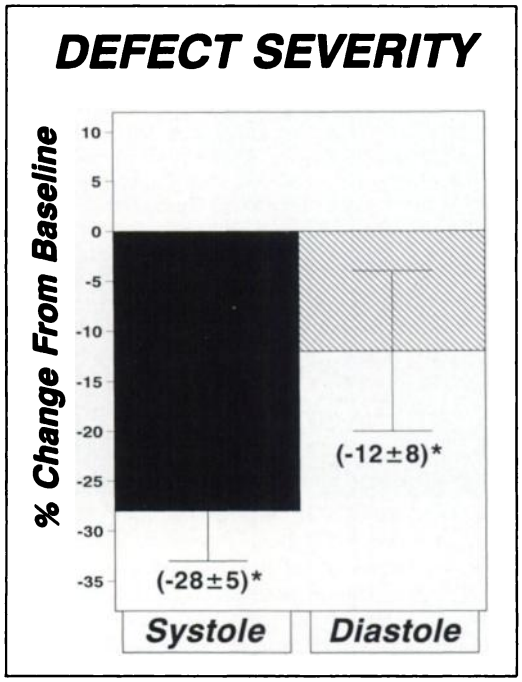

FIGURE 4. This figure illustrates the average percent change in the defect severity (abnormal counts divided by normal counts) between baseline-rest and occlusion images (n = 10). Abnormal segmental contraction per se caused an apparent "perfusion" defect on myocardial images at systole and diastole [(*) $p < 0.01$]. Defects on systolic images were more severe than on diastolic images ($p < 0.01$).

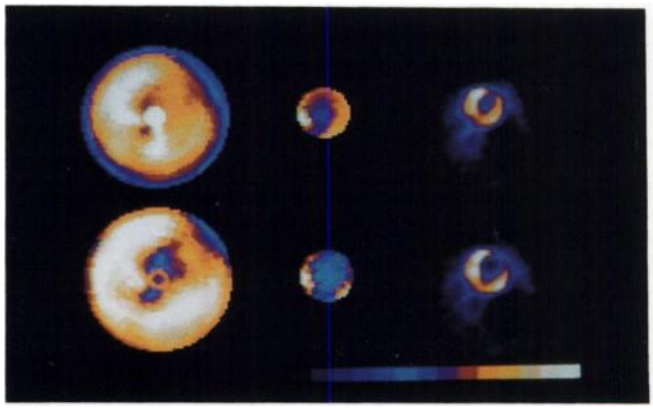

FIGURE 5. Ungated acquisition. This figure compares the bull's-eye images (left column), CAP displays (middle column) and corresponding transaxial slices (right column) from one subject. (Top row) Baseline-rest images were acquired during normal segmental contraction. (Bottom row) Occlusion images were acquired during abnormal segmental contraction. Abnormal segmental contraction per se caused an apparent "perfusion" defect on ungated SPECT myocardial perfusion images.

A great deal of clinical work with ^{99m}Tc-sestamibi has focused on the use of count changes during gated studies as a means of identifying changes in myocardial wall thickness as an index of segmental function (*18–22*). The relationship between count change and thickening follows from the work of Hoffman et al. (*23*) who showed, for an object size smaller than the resolution of the imaging system, that reconstructed count density is related to the size of the object. Myocardial wall thicknesses (values on the order of 10 mm) are less than the SPECT resolution (approximately 16 mm FWHM) in this experiment. Thus, we would predict that an increase of the count value in a maximum count circumferential profile between diastole and systole would occur in myocardial regions with normal or mildly reduced systolic wall function (region perfused by the LCx in the occlusion protocol). Conversely, regions with little or absent systolic wall thickening (abnormal region perfused by LAD in the occlusion protocol) should show little if any count change between systole and diastole. Thus, the absence of systolic wall thickening in one myocardial region (i.e., LAD), in conjunction with normal or mildly reduced wall thickening in other areas of the same heart (i.e., LCx), would produce an apparent "perfusion" defect at systole since, relatively fewer counts at systole, compared to baseline, would be apparent in the region dependent on blood flow from the occluded (LAD) artery compared to the region perfused by the LCx. DiBella et al. (*24*) have presented results from a three-dimensional computer simulation model of SPECT imaging of the heart which includes the effects of SPECT resolution. In agreement with the dog data presented here and the analysis of Hoffman et al. (*23*), their model results predict the appearance of "artifactual" defects in thinner versus thicker myocardial wall segments. In agreement with our

experimental results, defects are predicted to be more severe in systolic images compared to diastolic images acquired during occlusion (*24*).

Although we have used ^{99m}Tc-sestamibi as an imaging agent, abnormal segmental contraction in association with the effects of limited SPECT resolution discussed above, should similarly influence images acquired with any isotope residing in the myocardium. Accordingly, the results of this study may have several important implications for interpretation of clinical myocardial perfusion imaging. In particular,

1. The consequences of the influence of systole on ungated myocardial perfusion images (as shown in Fig. 5) may include the creation of defects in "perfusion" images that actually are due to abnormalities in segmental contraction rather than to heterogeneity in perfusion.
2. End-diastolic imaging was a better indicator of myocardial perfusion per se than end-systolic imaging. This observation follows directly from our data indicating that the end-systolic image is influenced to a greater extent by abnormal left ventricular contraction than the end-diastolic image ($p < 0.01$).

CONCLUSION

Abnormal segmental contraction can create apparent abnormalities on SPECT myocardial perfusion images. Accordingly, because of the intrinsic limitations of spatial resolution in SPECT imaging, apparent "perfusion" defects represent an integrated result of the combination of blood flow and segmental contraction heterogeneity.

ACKNOWLEDGMENTS

Supported by an American Heart Association/Georgia Affiliate Grant-in-aid, Marietta, Georgia and the Carlyle Fraser Heart Center, Atlanta, Georgia.

Presented at the 40th Annual Meeting of the Society of Nuclear Medicine, Toronto, Ontario, Canada, June 1993.

REFERENCES

1. Beller GA. Diagnostic accuracy of thallium-201 myocardial perfusion imaging. *Circulation* 1991;84(suppl I):11–16.
2. Pohost GM, Zir LM, Moore RH, McKusick KA, Guiney TE, Beller GA. Differentiation of transiently ischemic from infarcted myocardium by serial imaging after a single dose of thallium-201. *Circulation* 1977;55:294–302.
3. Braunwald E, Kloner RA. The stunned myocardium: prolonged post-ischemic ventricular dysfunction. *Circulation* 1982;66:1146–1149.
4. Gewirtz H, Grotte GJ, Strauss HW, et al. The influence of LV volume and wall motion on myocardial images. *Circulation* 1979;59:1172–1177.
5. Parodi AV, Schelbert HR, Schwaiger M, Hansen H, Selin C, Hoffman EJ. Cardiac emission computed tomography: estimation of regional tracer concentrations due to wall motion abnormality. *J Comput Assist Tomogr* 1984; 8:1083–1092.
6. Alderson PO, Wagner HN, Gomez-Moeiras JJ, et al. Simultaneous detection of myocardial perfusion and wall motion abnormalities by cinematic thallium-201 imaging. *Radiology* 1978;127:531–533.
7. Okada R, Glover D, Gaffney T, Williams S. Myocardial kinetics of ^{99m}Tc hexakis-2-methoxy-2-methylpropyl isonitrile. *Circulation* 1988;77:491–498.
8. Liu P, Houle S, Mills L, Dawood F. Kinetics of ^{99m}Tc MIBI uptake and clearance in ischemia-reperfusion: comparison with ^{201}Tl. *Circulation* 1987; 76:IV-216.
9. Li QS, Solot G, Frank TL, Wagner HN Jr, Becker LCV. Myocardial redistribution of technetium-99m-methoxy isobutyl isonitrile (sestamibi). *J Nucl Med* 1990;31:1069–1076.
10. Theroux P, Franklin D, Ross J Jr, Kemper WS. Regional myocardial function during acute coronary occlusion and its modification by pharmacologic agents in dogs. *Circ Res* 1974;34:896–908.
11. Vatner SF. Correlation between acute reduction in blood flow and function on conscious dogs. *Circ Res* 1980;47:201–207.
12. Gallagher KP, Osakada G, Hess OM, Koziol JA, Kemper WS, Ross J Jr. Subepicardial segmental function during coronary stenosis and the role of myocardial fiber orientation. *Circ Res* 1982;50:352–359.
13. Sasayama S, Franklin D, Ross Jr. J, Kemper WS, McKown D. Dynamic changes in left ventricular wall thickness and their use in analyzing cardiac function in the conscious dog. *Am J Cardiol* 1976;38:870–879.
14. Leon AR, Eisner RL, Martin SE, et al. Comparison of SPECT thallium-201 and SPECT ^{99m}Tc-sestamibi myocardial perfusion imaging in dogs. *J Am Coll Cardiol* 1992;20:1612–1625.
15. Boyers AS, Eisner RL, Chu TH, Oates JA, Curien B, Patterson RE. Quantitative analysis of myocardial perfusion scans with 3-D display [Abstract]. *J Nucl Med* 1990;31:808.
16. Eisner RL, Martin SE, Leon AR, et al. Inhomogeneity of gated and ungated SPECT technetium-99m-sestamibi bull's-eyes in normal dogs: comparison with thallium-201. *J Nucl Med* 1993;34:281–287.
17. Machac J, Levin H, Balk E, Horowitz SF. Computer modeling of planar myocardial perfusion imaging: effect of heart rate and ejection fraction on wall thickness and chamber size. *J Nucl Med* 1986;27:653–659.
18. Marcassa C, Marzullo P, Pandi O, Sambuceti G, L'Abbate A. A new method for noninvasive quantitation of segmental myocardial thickening using ^{99m}Tc-sestamibi: results in normal subjects. *J Nucl Med* 1990;31:173–177.
19. Ziffer JA, Cooke CD, Folks RD, Lapidus AS, Alzaraki NP, Garcia E. Quantitative myocardial thickening assessed with sestamibi: evaluation of a count-based method [Abstract]. *J Nucl Med* 1991;32:1006.
20. Mochizuki T, Murase K, Fujiwara Y, Tanada S, Hamamoto K, Tauxe W. Assessment of systolic thickening with ^{201}Tl ECG-gated SPECT: a parameter of local left ventricular function. *J Nucl Med* 1991;32:1496–1500.
21. Maisey MN, Mistry R, Sowton E. Planar imaging techniques used with technetium-99m sestamibi to evaluate myocardial ischemia. *Am J Cardiol* 1990;66:47E–54E.
22. Verzijlbergen JF, Suttorp MJ, Ascoop CA, et al. Combined assessment of technetium-99m sestamibi planar myocardial perfusion images at rest and during exercise with rest/exercise left ventricular wall motion studies evaluated from gated myocardial perfusion studies. *Am Heart J* 1992;123:59–68.
23. Hoffman EJ, Huang SC, Phelps ME. Quantitation in positron emission computed tomography: 1. Effect of object size. *J Comput Assist Tomography* 1979;3:299–308.
24. DiBella E, Boyers AS, Chu TH, Patterson RE, Eisner RL. Computer simulation of false myocardial perfusion defects [Abstract]. *J Nucl Med* 1993;34:29P.